Short-Range Disorder in TeO₂ Melt and Glass

O. L. G. Alderman,*,[†,#] C. J. Benmore,[‡] S. Feller,[§] E. I. Kamitsos,[∥] E. D. Simandiras,[∥] D. G. Liakos,[⊥] M. Jesuit,[§] M. Boyd,[§] M. Packard,[§] and R. Weber[†,‡]

[†]Materials Development, Inc., Arlington Heights, Illinois 60004, United States
[‡]X-Ray Science Division, Advanced Photon Source, Argonne National Laboratory, Argonne, Illinois 60439, United States
[§]Department of Physics, Coe College, Cedar Rapids, Iowa 52402, United States
[∥]National Hellenic Research Foundation, 48 Vassileos Constantinou Avenue, 11635 Athens, Greece
[⊥]Max-Planck-Institut für Kohlenforschung, Kaiser-Wilhelm-Platz 1, 45470 Mülheim an der Ruhr, Germany

S *Supporting Information*

ABSTRACT: High-resolution X-ray pair distribution functions for molten and glassy TeO₂ reveal coordination numbers $n_{TeO} \approx 4$. However, distinct from the known α-, β-, and γ-TeO₂ polymorphs, there is considerable short-range disorder such that no clear cutoff distance between bonded and nonbonded interactions exists. We suggest that this is similar to disorder in δ-TeO₂ and arises from a broad distribution of asymmetric Te−O−Te bridges, something that we observe becomes increasingly asymmetric with increasing liquid temperature. Such behavior is qualitatively consistent with existing interpretations of Raman scattering spectra, and equivalent to temperature-induced coordination number reduction, for sufficiently large cutoff radii. Therefore, TeO₂ contains a distribution of local environments that are, furthermore, temperature dependent, making it distinct from the canonical single-oxide glass formers. Our results are in good agreement with high-level *ab initio* cluster calculations.
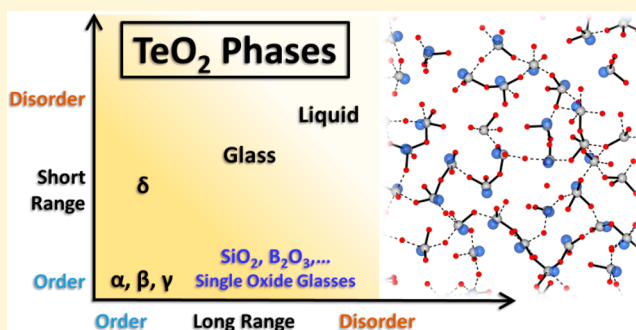
Tellurium dioxide is an enigmatic compound with several known crystalline polymorphs, which can, reluctantly, be melt-quenched to form a single-oxide glass in bulk.[1] This latter property is shared by only a handful of oxides (B₂O₃, SiO₂, GeO₂, P₂O₅, V₂O₅, As₂O₃, Sb₂O₃, TeO₂) and of these only the latter three are based on lone-pair cations with nonbonding s-electron pairs. Stereochemical activity of the cationic lone pairs leads to highly asymmetrical coordination polyhedra with just a few short, strong bonds to oxygen forming on the opposite side of the cation. As such, at least the first two of Zachariasen's topological rules[2] for glass formation are satisfied in the "lone-pair oxide" glasses. While diffraction measurements on the lone-pair oxide glasses indicate well-defined trigonal pyramidal coordination polyhedra for As³⁺ [3] and Sb³⁺,[4] the coordination of Te⁴⁺ to oxygen is less clear-cut, with a range of values between $3.6 < n_{TeO} \lesssim 4.0$ reported.[5−10] The differences are important because $n_{TeO} < 4$ implies the existence of nonbridging, or terminal, Te=O groups, the fraction of oxygen in such groups being $f_{TO} = 2 − n_{TeO}/2 = 2 − n_{OTe}$.[5] Clarifying the local coordination environment in TeO₂ glass is therefore important for understanding structure−property relationships in tellurite glasses and enabling property prediction and optimization. Indeed, considering their wide infrared transmission windows, high refractive indices, and nonlinear optical susceptibilities,[11] glasses based on TeO₂ are promising materials for various optical devices, including photonic switches. The optical nonlinearity in particular is strongly influenced by the local structural arrangements.[12,13]

It can often be conducive to consider the melt structure alongside that of the ambient glass,[8,14] especially considering that glasses are always derived by (sufficiently rapid) cooling from the liquid state. The structure and transport properties of the (supercooled) liquid phase also control crystal growth and are required for its optimization.[15] Moreover, molten oxides are important materials in their own right as high-temperature hermetic seals and oxide ion conducting electrolytes for fuel cells and gas separation membranes, including those based on molten TeO₂.[16,17] Although the structure of molten TeO₂ is less well studied than that of the glass, a recent Raman spectroscopic investigation[8] has been interpreted in terms of a declining Te−O coordination number with increasing temperature, along with a concomitant increase in the number of Te=O doubly bonded terminal oxygen groups. *Ab-initio* molecular dynamics (MD) simulations[18] support this interpretation to some extent, although the liquid states studied were highly pressurized due to the use of a fixed density, something that likely suppresses the coordination decrease.

The existence of Te=O groups in TeO_2 glass, based on values of $n_{TeO} < 4$,[5] has been somewhat contentious[6] and it has been recognized that the method of determination of n_{TeO},[9] as well as the definition of what constitutes a bonded interaction[6] must be considered.

In this Letter we use high-energy X-ray diffraction to obtain high-resolution pair distribution functions for both molten and glassy TeO_2. X-ray diffraction is relatively less sensitive to scattering contributions from O—O pairs than is neutron diffraction,[5,10] and in this way, it is more sensitive to the Te—O distance distribution, especially the longer Te—O interatomic distances, as well as those of Te—Te pairs. We are able to demonstrate unequivocally that the short Te—O bonds present in TeO_2 glass become shorter, and stronger, in the high-temperature liquid, something that is typically associated with a reduction in coordination number,[19,20] and which is qualitatively consistent with interpretations of Raman scattering spectra.[8] This has implications for the MD modeling of TeO_2 glass, because the hyperquenching necessitated by the short accessible time scales may freeze-in an unrealistically low Te—O coordination number. Furthermore, we show that a highly asymmetric Te—O distance distribution persists in the liquid state, such that no clear cutoff distance between bonded and nonbonded interactions exists. We support our findings with high-level *ab initio* relaxations of amorphous TeO_2 clusters and discuss their consequences on the debate concerning TeO_2 glass structure. We favor a qualitative description within which $n_{TeO} \approx 4$ but with a wide distribution of asymmetric Te—O—Te bridges that becomes increasingly asymmetric with increasing temperature in the liquid, effectively lowering n_{TeO} below that of the glass, for sufficiently large cutoff radii.

High-energy X-ray diffraction measurements were made at beamline 6-ID-D of the Advanced Photon Source. TeO_2 glass was prepared as described elsewhere,[1,7] followed by grinding to a powder with an agate pestle and mortar. The fine powder was loaded into a thin-walled borosilicate glass capillary of 1.5 mm internal diameter and the diffraction pattern was recorded using an incident beam energy of 100.36 keV and a flat-panel Varex 4343CT detector (2880×2880 pixels of 150 μm $\times$ 150 μm) for a total of 15 min. An empty capillary was also measured for the purpose of background subtraction. The sample-to-detector distance of 346.9 mm was calibrated by measurement of a sample of NIST standard CeO_2. For the study of molten TeO_2, polycrystalline samples were first formed from TeO_2 powder into beads of ~3 mm diameter using a laser hearth melter.[21] A 53.93 mg sample was floated on a stream of pure O_2 gas in a converging-diverging conical nozzle aerodynamic levitator.[19,20] A 10.6 μm CO_2 gas laser was weakly focused onto the top of the sample as the heating source, and the X-ray beam (200 μm high $\times$ 500 μm wide) passed through this upper portion of the levitated molten droplet. X-rays of 89.63 keV were used, along with a PerkinElmer XRD1621 detector (2048×2048 pixels of 200 μm $\times$ 200 μm) for a measurement duration of 42 s. The empty levitator with gas flowing was also measured for the purpose of background subtraction, and the sample-to-detector distance of 345.3 mm was calibrated by measurement of a sample of NIST standard CeO_2. Temperature measurement was made using a 1.55 μm optical pyrometer; however, sample melting was clearly observed at apparent temperatures of ~800 K, far lower than the known melting point of $T_m = 1005$ K. Although the spectral emissivity of TeO_2 has been reported to be as low as

0.31,[15] this does not account for such a low apparent temperature, and partial infrared transparency of the sample at 1.55 μm is implied. We estimate our measurement temperature to be ~1100 K since a moderate amount of overheating (above T_m) is required to overcome temperature gradients within the partially molten sample and obtain complete melting. Separate experiments using a 5 μm pyrometer were found to be consistent with an emissivity of 0.343, based on the temperature of recalescence observed during crystallization upon cooling. The temperature of the fully molten droplet calculated with this value for the emissivity was 1134 ± 46 K; however, it is not clear if partial transparency, even at 5 μm, does not also contribute to the low apparent temperature. Retention of TeO_2 stoichiometry is supported by the white (not discolored) appearance of the recovered solidified bead within the levitator, and by X-ray diffraction of the same, with Bragg peak positions matching those expected for the thermodynamically stable α-TeO_2 polymorph (Figure S1). It is also worth noting that separate experiments performed with high-purity argon as the levitation gas showed recovered sample discoloration to dark yellow and enhanced sample mass losses (10.1% over 20 s) compared to that in oxygen (3.8% over 42 s), and diffraction data (100.32 keV) could not be effectively normalized by assuming a stoichiometric TeO_2 composition. These observations, along with the known redox behavior of tellurium,[22] suggest partial reduction of Te^{4+} to metallic Te^0 in the melt in argon atmosphere. Diffraction patterns were corrected and reduced as described elsewhere[20] to obtain the X-ray structure factors $S(Q)$ plotted in Figure 1 and total correlation functions $T(r)$ presented in Figure 2.
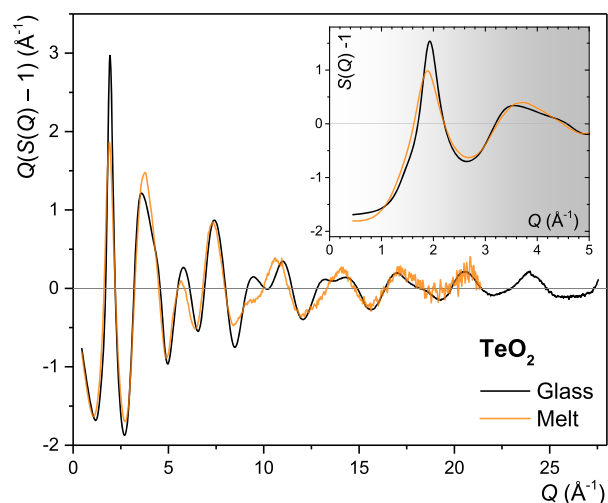
Figure 1. X-ray interference functions, $Q(S(Q) - 1)$, for molten and glassy TeO_2. The structure factors, $S(Q) - 1$, are shown in the inset for $Q \leq 5$ Å^{-1}, where the shift of the first diffraction peak to lower Q in the melt is more clearly visible.

In order to quantitatively interpret total scattering diffraction data the bulk density is required.[20] For TeO_2 glass we take the density to be 5.65 gcm^{-3}, in good agreement with direct measurements[1,7,9] as well as linear extrapolation of binary tellurite glass densities.[23] For molten TeO_2 we are aware of only a single, unverified value of 5.5 g cm^{-3} at an unspecified temperature.[15] On the basis of the thermal expansion of paratellutire (α-TeO_2),[24] however, a lower melt density might
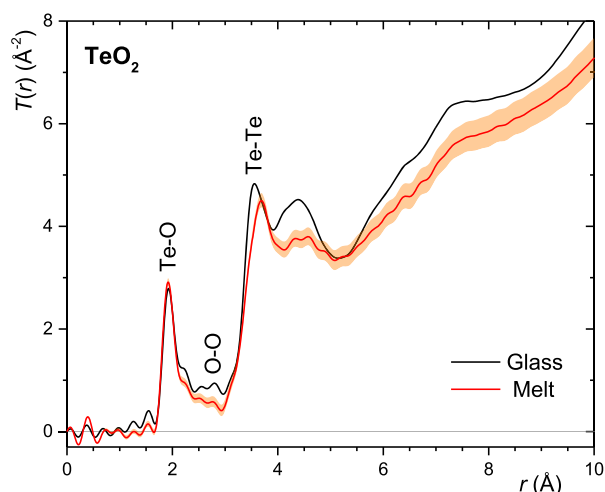
Figure 2. X-ray total correlation functions obtained by the sine Fourier transform of the interference functions of Figure 1, using a Q_{max} = 21.39 Å^{-1} and the step modification function, which yields the highest possible resolution. The shaded region represents the range of results based on a melt density of 5.09 ± 0.27 g cm^{-3}.

be expected; see Figure S2. As such, we analyze our data for molten TeO$_2$ for a range of densities of 5.09 ± 0.27 g cm^{-3}.

We note that a melt density lower than that of the glass is supported by the shift of the first diffraction peak (FDP) to lower Q in the melt, Figure 1 (inset). Lower Q corresponds to a larger real-space periodicity, in this case of the Te−Te pair distribution, which can be seen in the $D(r)$ of Figure S4, as well as in the increased nearest-neighbor Te−Te distance in the melt clearly evident in Figure 2. If the melt were denser than the glass, the TeO$_2$ (supercooled) liquid would have to display negative thermal expansion, which would put it into the category of anomalous liquids such as supercooled liquid silica or water.

In order to gain detailed insight into the distribution of Te−O distances in molten and glassy TeO$_2$, we deconvolute the $T(r)$ and obtain the radial distribution function RDF$_{TeO}(r)$ = $c_O r T_{TeO}(r)$ as described in the Supporting Information and plotted in Figure 3. By combining our X-ray diffraction data for TeO$_2$ glass with published neutron diffraction data,[5] we are able to show that the contribution from the O−O pair term is negligible for $r \lesssim$ 2.4 Å, Figure S7, and small beyond this. Thus, the running coordination numbers $n_{TeO}(r)$, also plotted in Figure 3, truly correspond to the Te−O coordination number up to $r \approx$ 2.4 Å. Clearly, the $n_{TeO}(r)$ show no indication of a plateau and therefore no unambiguous delineation between bonded and nonbonded coordination shells. On the basis of the X-ray-neutron difference function, Figure S7, this conclusion holds for the glass out to at least 3.0 Å (where the Te−Te pair term starts to contribute) and is consistent with our *ab initio* calculations of the structure of amorphous TeO$_2$ clusters (Figure 3, and see the Supporting Information). This is in contrast to the known structures of the α-, β-, and γ-TeO$_2$ crystalline polymorphs, all of which show a plateau at $n_{TeO}(r \approx$ 2.4 Å) = 4, even when accounting for thermal and instrumental broadening effects (see, e.g., γ-TeO$_2$ in Figure 3). This difference between the amorphous and crystalline structures is likely due to the presence of a distribution of local coordination environments in liquid and glassy TeO$_2$, perhaps similar to that expected in the disordered δ-TeO$_2$ phase.[25,26]
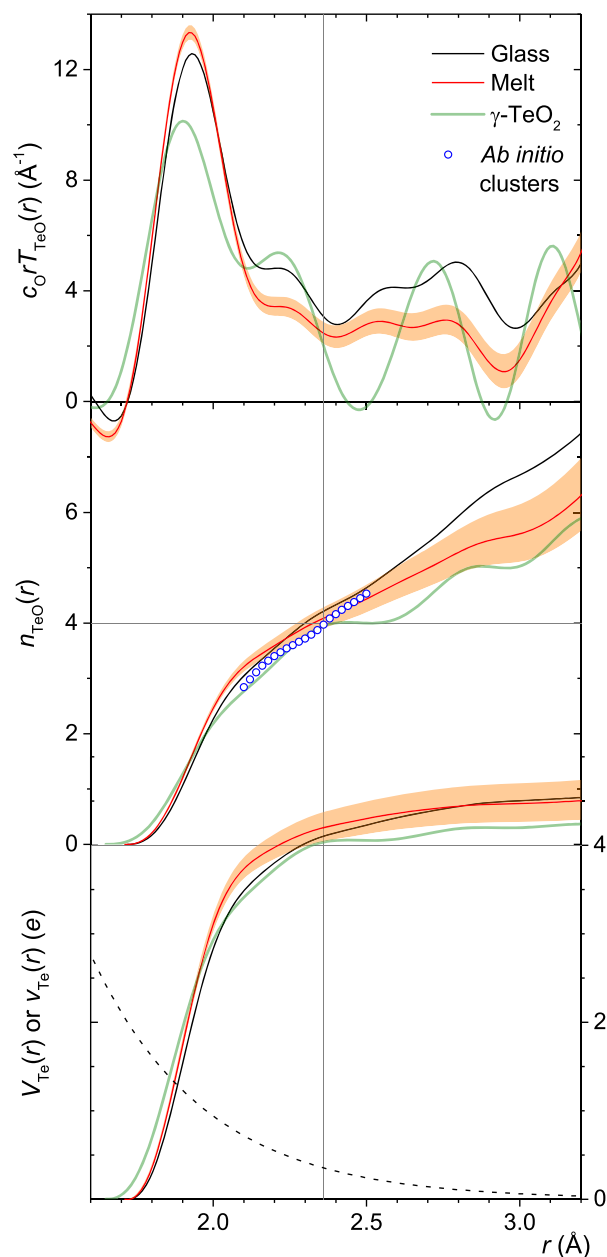
Figure 3. Upper panel: X-ray radial distribution functions (RDFs) with the Q-dependent Te−O pair weighting divided out, prior to sine Fourier transform of the interference functions of Figure 1, using Q_{max} = 21.39 Å^{-1}. Also shown is the Te−O RDF in γ-TeO$_2$[28] calculated using the XTAL program[29] and convolved with the same instrumental broadening as the X-ray data and a thermal broadening of 0.07 Å. Middle panel: running Te−O coordination numbers ($n_{TeO}(r)$), obtained by integration of the RDFs with the lower limit of the integral set to the zero-crossing at ∼1.72(1) Å. Results of our *ab initio* amorphous cluster calculations are also shown (blue circles; see Supporting Information). Lower panel: running bond valence sums for Te obtained similarly to the $n_{TeO}(r)$, but after weighting by $v_{Te}(r)$ = $\exp(R_{TeO} − r)/b$ (dashed line) prior to integration.[30]

There are some subtle but clear differences between the bonding in glassy and molten TeO$_2$. By peak fitting[27] to the $T(r)$ of Figure 2, a slightly shorter peak bond distance of 1.919(2) Å can be found for the melt, compared to 1.926(1) Å in the glass. This is the opposite to what would be expected for *isotropic* thermal expansion of a fixed coordination environment. However, the long Te−O bonds will experience greater

anharmonicity in their thermal variations, which can lead to an overall contraction of the short bonds to compensate. At a certain point, if the long bonds become long and weak enough, they will no longer "qualify" as bonded interactions and the overall effect is a drop in coordination number. This is exactly what has been suggested on the basis of detailed analysis of the Raman spectra of molten and glassy TeO_2.[8] The question as to how asymmetric a Te−O−Te bridge can become before it is considered broken to form a Te═O group may not have an unambiguous answer, and this has likely contributed to the debate over the structure of TeO_2 glass.

Taking the somewhat arbitrary cutoff radius of 2.36 Å (similar to that used elsewhere),[5,9,10,18] we obtain $n_{TeO}(2.36 \text{ Å})$ = 4.22 in the glass and $n_{TeO}(2.36 \text{ Å})$ = 4.09 ± 0.20 in the melt. Thus, the coordination number is close to 4 with only a hint that it may be lower in the melt, especially considering that the statistical uncertainties are ~0.1. However, using a single arbitrary cutoff can be misleading. Looking at the running $n_{TeO}(r)$ in Figure 3 it is clear that the value initially rises more steeply for the melt than for the glass, crossing over somewhere between 2.15 and 2.55 Å such that the coordination number is larger in the glass only for a sufficiently large cutoff radius. This means that the longer Te−O bonds are more important for satisfying the bonding requirements of Te^{4+} in the glass than in the melt, where the shorter bonds are stronger and more dominant.

Another way to consider the relative importance of bonds is through the running bond-valence sum:[30]

$$V_{Te}(r) = c_O \int_0^r r' \text{data files } T_{TeO}(r') e^{(R_{TeO} - r'/b)} \, dr' \qquad (1)$$

Equation 1 is identical to the definition of the running coordination number, except for the inclusion of the bond-valence weighting factor, $v_{Te}(r) = \exp(R_{TeO} - r)/b$ (Figure 3), where $R_{TeO} = 1.977$ Å is the bond-valence parameter and $b = 0.37$ Å is a universal empirical constant.[31] The results from applying eq 1 to our data are shown in Figure 3. It is clearly evident that the bond-valence sum reaches the formal tellurium valence ($V_{Te} = 4$) at shorter radial cutoff in the melt than in the glass, and longer bonds are more important in the glass for bringing $V_{Te}(r)$ up to a similar asymptotic value as in the liquid. We note that bond-valence parameters are expected to increase with temperature[14,20] due to thermal expansion and that this would enhance the difference in $V_{Te}(r)$ between liquid and glass, as would any increase in the melt density.

In summary the TeO_2 liquid-glass system is distinct from other single-oxide glass formers, particularly the canonical network formers B_2O_3, SiO_2, GeO_2, and P_2O_5, in that its structure incorporates short-range disorder. This is likely similar to that expected in disordered crystalline δ-TeO_2[25,26] and leads to a poorly defined coordination number ($n_{TeO} \approx 4$), which has contributed to apparent disagreement in the literature. We propose that the disorder manifests as a distribution of asymmetric Te−O−Te bridges and that higher temperatures enhance this asymmetry. The latter is qualitatively consistent with coordination number reduction, as inferred from Raman spectroscopy,[8] although this is only quantitatively observed by diffraction measurements when evaluating n_{TeO} out to sufficiently large cutoff radii. The extent to which doubly bonded Te═O groups are present is therefore somewhat subjective in that these may simply be oxygen ions within highly asymmetrical Te−O−Te bridges.

ASSOCIATED CONTENT

Ⓢ Supporting Information

The Supporting Information is available free of charge at https://pubs.acs.org/doi/10.1021/acs.jpclett.9b03231.

Diffraction patterns of polycrystalline samples prior to and post melting experiments, summary of density data for TeO_2 phases and estimates for the liquid, comparison of independently measured X-ray diffraction data sets for TeO_2 glass, $D(r)$ functions showing medium range correlations out to 20 Å; description of the derivation of the radial distribution functions, running Te−O coordination numbers and bond-valence sums; description of the derivation of X-ray-neutron difference functions used for eliminating the contribution of O−O correlations from the diffraction data for TeO_2 glass; computational details for amorphous TeO_2 cluster production and analysis; exemplary relaxed structures of the clusters; (PDF)

X-ray $S(Q) − 1$ data file for the TeO_2 melt (TXT)

X-ray $S(Q) − 1$ data file for the glass (TXT)

AUTHOR INFORMATION

Corresponding Author

*o.alderman@gmail.com.

ORCID Ⓞ

O. L. G. Alderman: 0000-0002-2342-811X

E. I. Kamitsos: 0000-0003-4667-2374

D. G. Liakos: 0000-0002-4252-2881

Present Address

#ISIS Facility, Rutherford Appleton Laboratory, Chilton, Didcot, Oxon OX11 0QX, U.K.

Notes

The authors declare no competing financial interest.

REFERENCES

(1) Tagiara, N. S.; Palles, D.; Simandiras, E. D.; Psycharis, V.; Kyritsis, A.; Kamitsos, E. I. Synthesis, thermal and structural properties of pure TeO_2 glass and zinc-tellurite glasses. *J. Non-Cryst. Solids* **2017**, *457*, 116−125.

(2) Zachariasen, W. H. The Atomic Arrangement in Glass. *J. Am. Chem. Soc.* **1932**, *54*, 3841−3851.

(3) Mei, Q.; Hart, R. T.; Benmore, C. J.; Amin, S.; Leinenweber, K.; Yarger, J. L. The structure of densified As_2O_3 glasses. *J. Non-Cryst. Solids* **2007**, *353*, 1755−1758.

(4) Orman, R. G. Characterisation of novel antimony (III) oxide-containing glasses. *Ph.D. Thesis*, University of Warwick, Coventry, 2010.

(5) Barney, E. R.; Hannon, A. C.; Holland, D.; Umesaki, N.; Tatsumisago, M.; Orman, R. G.; Feller, S. Terminal oxygens in amorphous TeO_2. *J. Phys. Chem. Lett.* **2013**, *4*, 2312−2316.

(6) Garaga, M. N.; Werner-Zwanziger, U.; Zwanziger, J. W.; DeCeanne, A.; Hauke, B.; Bozer, K.; Feller, S. Short-Range Structure of TeO_2 Glass. *J. Phys. Chem. C* **2017**, *121*, 28117−28124.

(7) Marple, M. A. T.; Jesuit, M.; Hung, I.; Gan, Z.; Feller, S.; Sen, S. Structure of TeO_2 glass: Results from 2D ^{125}Te NMR spectroscopy. *J. Non-Cryst. Solids* **2019**, *513*, 183−190.

(8) Kalampounias, A. G.; Tsilomelekis, G.; Boghosian, S. Glass-forming ability of TeO_2 and temperature induced changes on the structure of the glassy, supercooled, and molten states. *J. Chem. Phys.* **2015**, *142*, 154503.

(9) Gulenko, A.; Masson, O.; Berghout, A.; Hamani, D.; Thomas, P. Atomistic simulations of TeO_2-based glasses: interatomic potentials and molecular dynamics. *Phys. Chem. Chem. Phys.* **2014**, *16*, 14150−14160.

(10) Niida, H.; Uchino, T.; Jin, J.; Kim, S.-H.; Fukunaga, T.; Yoko, T. Structure of alkali tellurite glasses from neutron diffraction and molecular orbital calculations. *J. Chem. Phys.* **2001**, *114*, 459−467.

(11) El-Mallawany, R. A. *Tellurite glasses handbook: physical properties and data*; CRC Press, 2016.

(12) Noguera, O.; Suehara, S. High nonlinear optical properties in TeO_2-based materials: Localized hyperpolarisability approach. *Ferroelectrics* **2007**, *347*, 162−167.

(13) Jeansannetas, B.; Blanchandin, S.; Thomas, P.; Marchet, P.; Champarnaud-Mesjard, J. C.; Merle-Mejean, T.; Frit, B.; Nazabal, V.; Fargin, E.; Le Flem, G.; et al. Glass structure and optical nonlinearities in thallium(I) tellurium(IV) oxide glasses. *J. Solid State Chem.* **1999**, *146*, 329−335.

(14) Alderman, O. L. G.; Ferlat, G.; Baroni, A.; Salanne, M.; Micoulaut, M.; Benmore, C. J.; Lin, A.; Tamalonis, A.; Weber, J. K. R. Liquid B_2O_3 up to 1700K: X-ray diffraction and boroxol ring dissolution. *J. Phys.: Condens. Matter* **2015**, *27*, 455104.

(15) Veber, P.; Mangin, J. TeO_2 liquid phase: Viscosity measurements and evaluation of the thermal conductivity from crystal growth experiments. *Mater. Res. Bull.* **2008**, *43*, 3066−3073.

(16) Belousov, V. V.; Fedorov, S. V. A Novel Molten Oxide Fuel Cell Concept. *Fuel Cells* **2016**, *16*, 401−403.

(17) Belousov, V. V. Next-Generation Electrochemical Energy Materials for Intermediate Temperature Molten Oxide Fuel Cells and Ion Transport Molten Oxide Membranes. *Acc. Chem. Res.* **2017**, *50*, 273−280.

(18) Pietrucci, F.; Caravati, S.; Bernasconi, M. TeO_2 glass properties from first principles. *Phys. Rev. B: Condens. Matter Mater. Phys.* **2008**, *78*, 064203.

(19) Alderman, O. L. G.; Benmore, C. J.; Tamalonis, A.; Sendelbach, S.; Heald, S. M.; Weber, R. Continuous Structural Transition in Glass-Forming Molten Titanate $BaTi_2O_5$. *J. Phys. Chem. C* **2016**, *120*, 26974−26985.

(20) Alderman, O. L. G.; Benmore, C. J.; Lin, A.; Tamalonis, A.; Weber, J. K. R. Borate melt structure: Temperature dependent B-O bond lengths and coordination numbers from high-energy x-ray diffraction. *J. Am. Ceram. Soc.* **2018**, *101*, 3357−3371.

(21) Richard Weber, J. K.; Felten, J. J.; Nordine, P. C. Laser hearth melt processing of ceramic materials. *Rev. Sci. Instrum.* **1996**, *67*, 522−524.

(22) Machado, T. M.; Silva, M. A. P. The reduction of tellurium in binary glasses in the system TeO_2-Sb_2O_3. *Mater. Chem. Phys.* **2017**, *201*, 86−91.

(23) Barney, E. R.; Hannon, A. C.; Holland, D.; Umesaki, N.; Tatsumisago, M. Alkali environments in tellurite glasses. *J. Non-Cryst. Solids* **2015**, *414*, 33−41.

(24) Krishna Rao, K. V.; Iyengar, L. X-ray studies on the thermal expansion of tellurium dioxide. *J. Mater. Sci.* **1972**, *7*, 295−297.

(25) Mirgorodsky, A. P.; Merle-Méjean, T.; Champarnaud, J. C.; Thomas, P.; Frit, B. Dynamics and structure of TeO_2 polymorphs: model treatment of paratellurite and tellurite; Raman scattering evidence for new γ- and δ-phases. *J. Phys. Chem. Solids* **2000**, *61*, 501−509.

(26) Gulenko, A. Structural study of amorphous TeO_2 and disordered δ-TeO_2 phase by molecular dynamics simulations. *Ph.D. Thesis*, Université de Limoges, 2014.

(27) Hannon, A. C. *PFIT Correlation Function Fitting Software.* http://www.alexhannon.co.uk/ (accessed Jan 18 2011).

(28) Weil, M. Redetermination of the γ-form of tellurium dioxide. *IUCrData* **2017**, *2*, x171757.

(29) Hannon, A. C. *RAL-93−063: XTAL: A program for calculating interatomic distances and coordination numbers for model structures*; Rutherford Appleton Laboratory, 1993.

(30) Hannon, A. C. Bonding and structure in network glasses. *J. Non-Cryst. Solids* **2016**, *451*, 56−67.

(31) Brese, N. E.; O'Keeffe, M. Bond-valence parameters for solids. *Acta Crystallogr., Sect. B: Struct. Sci.* **1991**, *47*, 192−197.